Preprints of the 23rd IFAC World Congress
Busan, Republic of Korea, August 23-28, 2026

Modelling, Parameter Identification and Nonlinear Control of a Proton Exchange Membrane Fuel Cell for Maritime Use [2]

Halit Ege Ceyhun [*,1] **Udai Shipurkar** [**] **Lindert Van Biert** [*]
Rudy R. Negenborn [*] **Andrea Coraddu** [*]

[*] *Delft University of Technology, Delft, The Netherlands (e-mail: {h.e.ceyhun, l.vanbiert, r.r.negenborn, a.coraddu}@tudelft.nl).*
[**] *Maritime Research Institute Netherlands, Wageningen, The Netherlands (e-mail: u.shipurkar@marin.nl)*

Abstract: Zero-emission maritime power systems require advanced control strategies for Proton Exchange Membrane (PEM) fuel cells. This study develops a physics-based, control-oriented dynamic model of a PEM fuel cell. Model parameters are optimally identified for an average cell using experimental data from a system comprising four stacks, each with 96 cells. Two nonlinear controllers — Dynamic Feedback Linearization (DFL) and an Integral Sliding Mode Controller (ISMC) — are implemented and compared. Results show faster transients with DFL, while ISMC provides improved robustness for power tracking.

Keywords: Modelling, Identification and Control in Marine Systems; Power and Propulsion in Marine Systems; Automatic Control, Optimisation, Real-time Operations in Transportation

1. INTRODUCTION

Strict maritime emission regulations IMO (2020) have increased interest in alternative fuels, energy storage systems, and energy management strategies (EMS) Coraddu et al. (2025); Van Biert et al. (2016). Among these, Proton Exchange Membrane (PEM) fuel cells stand out due to their zero emissions, high efficiency, and fast start-up, making them attractive for maritime applications Elkafas et al. (2023). A representative single-line hybrid architecture, including battery packs and PEM fuel cells, is shown in Figure 1. According to Dall'Armi et al. (2023), PEM fuel cells (including high-temperature variants) are among the most mature and widely adopted technologies in maritime applications, accounting for approximately 77% of ongoing projects. As highlighted in Mylonopoulos et al. (2023), effective EMS development in the decarbonising maritime sector is closely linked to controller design and relies on accurate dynamic modelling. However, modelling these devices is challenging due to the interconnected, nonlinear dynamics among multiple variables.

Many models in the literature approximate PEM fuel cell dynamics using polarisation curves (voltage–current) or selected subsystems, often neglecting coupled electrochemical and thermodynamic phenomena. For control-oriented modelling, state-space formulations are preferred due to their systematic framework for controller design. PEM fuel cell control has been widely studied. Daud et al. (2017) and Wang et al. (2024) propose classifications of common control techniques, focusing mainly on Proportional–Integral–Derivative (PID) Control, Fuzzy Logic Control (FLC), Adaptive Control, and Model Predictive Control (MPC). These classifications emphasise the broad range of applicable approaches.

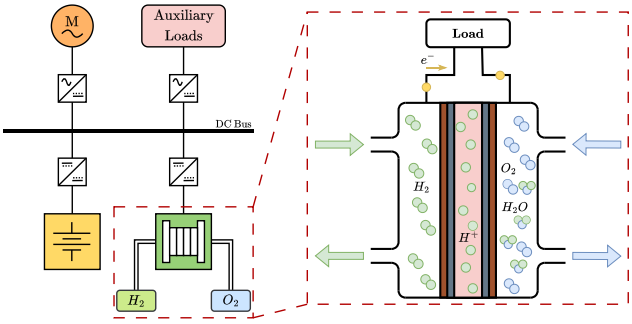


Fig. 1. PEM Fuel Cell - Battery Hybrid Diagram

Several modelling and control approaches for PEM fuel cell systems have been reported in the literature. Meidanshahi and Karimi (2012) developed a nonlinear dynamic model with Differential Evolution-based parameter optimisation, comparing PI and FLC for power regulation. A singular perturbation-based LQR approach decoupling fast and slow dynamics was proposed in Kodra and Zhong (2020). A comprehensive 16-state, 7-input automotive model capturing anode, cathode, membrane, and catalyst dynamics is presented in Ritzberger et al. (2020), with optimal parameter estimation via local linearization introduced in Ritzberger et al. (2021). Thermal management using a validated model with PI control is addressed in Zhang et al. (2020), while Rabbani and Rokni (2013) presents a complete system model incorporating gas flows, water crossover, and heat exchange. As a robust control approach, Sliding Mode Control (SMC) is applied for

[1] Corresponding author.
[2] This work was held under SH2IPDRIVE Project.

©2026 the authors. Accepted by IFAC for publication under a Creative Commons Licence CC-BY-NC-ND

flow rate and power regulation in Garcia-Gabin et al. (2010). Partial Feedback Linearization (PFL) with NSGA-II-optimised gains is employed in Alireza Abaspour (2014), and Li et al. (2009) combines exact feedback linearization with H_∞ robust control. MPC-based approaches are explored in Ziogou et al. (2018) and Chatrattanawet et al. (2017) within multi-objective optimisation frameworks.

Accurate parameter identification is critical for model-based control, as mismatches can severely affect system and actuator performance. A comparative analysis of optimisation methods for parameter estimation is presented in Korkmaz et al. (2024), while Santarelli et al. (2006) surveys polarisation curve parameter estimates.

2. CONTROL-ORIENTED MODELLING OF PEM FUEL CELL

A white-box modelling approach is adopted to enable systematic controller design, capturing the dominant dynamics at the lowest possible model order while preserving generalizability Coraddu et al. (2022). The following assumptions apply: water is produced solely at the cathode by neglecting back-diffusion and electro-osmotic drag. The thermal dynamics are 0D with uniform stack temperature. The water vapour partial pressure is limited by saturation, and the heat exchange with the gases is negligible.

2.1 System Dynamics of the PEM Fuel Cell

The PEM fuel cell model focuses on the oxidation and reduction reactions. The anode and cathode are supplied with pressurised hydrogen and oxygen, respectively. At the anode, hydrogen splits into protons and electrons. Electrons travel through the external circuit, satisfying the electrical power demand, while protons cross the membrane to the cathode, where they combine with oxygen to produce water. This exothermic process releases heat alongside the water byproduct:

$$\mathrm{H_2} \rightarrow 2\mathrm{H^+} + 2\mathrm{e^-}\,, \qquad \frac{1}{2}\mathrm{O_2} + 2\mathrm{H^+} + 2\mathrm{e^-} \rightarrow \mathrm{H_2O}\,. \quad (1)$$

Hence, the mass flow rates of hydrogen, oxygen and water are taken as the main contributors. The mass flow rates change in accordance with Faraday's Law of Electrolysis. Moreover, the net mass flow rates are given as follows:

$$\dot{m}_i = \dot{m}_{i,\mathrm{in}} + s_i\, \dot{m}_{i,\mathrm{reacted}} - \dot{m}_{i,\mathrm{out}}\,, \quad (2)$$

where $(i, s_i) \in \{(\mathrm{H_2}, -1),\ (\mathrm{O_2}, -1),\ (\mathrm{H_2O}, +1)\}$. The reacted and the outlet rates can be further expanded as follows:

$$\dot{m}_{i,\mathrm{reacted}} = \frac{I}{n_i F} M_i, \quad \dot{m}_{i,\mathrm{out}} = k_j (P_i - P_{\mathrm{out},j})\,, \quad (3)$$

where $(i, n_i, j) \in \{(\mathrm{H_2}, 2, \mathrm{a}),\ (\mathrm{O_2}, 4, \mathrm{c}),\ (\mathrm{H_2O}, 2, \mathrm{c})\}$, representing the molecule, the number of electrons participating the reaction and the chamber name as anode and cathode. Moreover, I is the current, F is the Faraday's constant, M_i are the hydrogen, oxygen and water molar masses, k_i are the linear nozzle constant of the anode and cathode sides, $P_{\mathrm{out},i}$ are the outlet pressure of the anode and cathode sides.

The thermal dynamics are primarily dependent on the reaction rate, process output and the heat removed by the cooling system. The following equation presents the 0D temperature dynamics of the cell as the combination of the reaction, the electrical and the removed heat.

$$\dot{T}_{\mathrm{cell}} = \frac{\frac{I}{2F}\,|\Delta H| - V_{\mathrm{cell}} I - h A_{\mathrm{cool}}\,(T_{\mathrm{cell}} - T_{\mathrm{cool}})}{m_{\mathrm{cell}} c_{\mathrm{p,cell}}}\,, \quad (4)$$

where m_{cell} and $c_{\mathrm{p,cell}}$ are the lumped cell mass and heat capacity, $|\Delta H|$ is the reaction enthalpy, h and A_{cool} are the convective heat transfer coefficient and cooling surface area, and T_{cell}, T_{cool} are the cell and coolant temperatures.

Partial pressures of hydrogen, oxygen, and water are considered as dynamic variables expressed by the ideal gas law. They directly affect electrochemical reactions and are explicitly reflected in the polarisation curve. The generic expression is presented as:

$$P_i = \frac{m_i R T_{\mathrm{cell}}}{M_i \nu_j}\,, \quad (5)$$

where $(i, j) \in \{(\mathrm{H_2}, \mathrm{a}),\ (\mathrm{O_2}, \mathrm{c}),\ (\mathrm{H_2O}, \mathrm{c})\}$, P_i are the partial pressures of hydrogen, oxygen and water, R is the universal gas constant and ν_j are the anode and cathode volumes respectively.

The cell voltage is the sum of the Nernst voltage, activation, concentration, and ohmic losses, which define the polarisation curve and thus the output power. The Nernst voltage represents the ideal open–circuit voltage. While activation and concentration losses dominate at low and high currents, ohmic losses act linearly across the full current range. The polarisation behaviour is expressed as follows:

$$\begin{aligned} V_{\mathrm{cell}} = {} & E^0 + \frac{R T_{\mathrm{cell}}}{2F} \ln\left(\frac{P_{\mathrm{H_2}}\sqrt{P_{\mathrm{O_2}}}}{P_{\mathrm{H_2O}}}\right) - \frac{R_\Omega I}{A_{\mathrm{m}}} \\ & - \sum_k \frac{R T_{\mathrm{cell}}}{n_i F \alpha_i} \ln\left(\frac{I}{A_{\mathrm{m}} i_{0,i}}\right) + \sum_k \frac{R T_{\mathrm{cell}}}{n_i F} \ln\left(1 - \frac{I}{A_{\mathrm{m}} i_{\mathrm{l},i}}\right)\,. \end{aligned} \quad (6)$$

$(k, n_k, \alpha_k, i_{0,k}, i_{\mathrm{l},k}) \in \{(\mathrm{a}, 2, \alpha_{\mathrm{a}}, i_{0,\mathrm{a}}, i_{\mathrm{l,a}}), (\mathrm{c}, 4, \alpha_{\mathrm{c}}, i_{0,\mathrm{c}}, i_{\mathrm{l,c}})\}$ with n_k the number of transferred electrons, α_k the charge transfer coefficient, $i_{0,k}$ and $i_{\mathrm{l},k}$ the exchange and limiting current densities for each side. E^0 is the open-circuit voltage, A_{m} the membrane surface area, R_Ω the ohmic resistance.

The nonlinear PEM fuel cell model takes input-affine form $\dot{x} = f(x) + g(x)u$, with the states and the inputs as:

$$\begin{aligned} x &= \left[m_{\mathrm{H_2}}\ m_{\mathrm{O_2}}\ m_{\mathrm{H_2O}}\ T_{\mathrm{cell}}\ P_{\mathrm{H_2}}\ P_{\mathrm{O_2}}\ P_{\mathrm{H_2O}}\ I\ V_{\mathrm{cell}}\right]^T\,, \\ u &= \left[\dot{m}_{\mathrm{H_2,in}}\ \dot{m}_{\mathrm{O_2,in}}\ \dot{m}_{\mathrm{H_2O,in}}\ T_{\mathrm{cool}}\ \dot{I}\right]^T\,. \end{aligned} \quad (7)$$

The system size is kept low-order to facilitate the future online optimisation-based energy management studies.

$$
\begin{aligned}
\dot{x}_1 &= u_1 - \frac{x_8}{2F} M_{\mathrm{H_2}} - k_{\mathrm{a}} \left(x_5 - P_{\mathrm{out,a}}\right) \,, \\
\dot{x}_2 &= u_2 - \frac{x_8}{4F} M_{\mathrm{O_2}} - k_{\mathrm{c}} \left(x_6 - P_{\mathrm{out,c}}\right) \,, \\
\dot{x}_3 &= u_3 + \frac{x_8}{2F} M_{\mathrm{H_2O}} - k_{\mathrm{c}} \left(x_7 - P_{\mathrm{out,c}}\right) \,, \\
\dot{x}_4 &= \frac{\frac{x_8}{2F} \left|\Delta H\right| - x_8 x_9 - h A_{\mathrm{cool}} \left(x_4 - u_4\right)}{m_{\mathrm{cell}} c_{\mathrm{p,cell}}} \,, \\
\dot{x}_5 &= \frac{\left(u_1 - \frac{x_8}{2F} M_{\mathrm{H_2}} - k_{\mathrm{a}} \left(x_5 - P_{\mathrm{out,a}}\right)\right) R x_4 + x_1 R \left(\frac{\frac{x_8}{2F} \left|\Delta H\right| - x_8 x_9 - h A_{\mathrm{cool}} \left(x_4 - u_4\right)}{m_{\mathrm{cell}} c_{\mathrm{p,cell}}}\right)}{M_{\mathrm{H_2}} \nu_{\mathrm{a}}} \,, \\
\dot{x}_6 &= \frac{\left(u_2 - \frac{x_8}{4F} M_{\mathrm{O_2}} - k_{\mathrm{c}} \left(x_6 - P_{\mathrm{out,c}}\right)\right) R x_4 + x_2 R \left(\frac{\frac{x_8}{2F} \left|\Delta H\right| - x_8 x_9 - h A_{\mathrm{cool}} \left(x_4 - u_4\right)}{m_{\mathrm{cell}} c_{\mathrm{p,cell}}}\right)}{M_{\mathrm{O_2}} \nu_{\mathrm{c}}} \,, \\
\dot{x}_7 &= \frac{\left(u_3 + \frac{x_8}{2F} M_{\mathrm{H_2O}} - k_{\mathrm{c}} \left(x_7 - P_{\mathrm{out,c}}\right)\right) R x_4 + x_3 R \left(\frac{\frac{x_8}{2F} \left|\Delta H\right| - x_8 x_9 - h A_{\mathrm{cool}} \left(x_4 - u_4\right)}{m_{\mathrm{cell}} c_{\mathrm{p,cell}}}\right)}{M_{\mathrm{H_2O}} \nu_{\mathrm{c}}} \,, \\
\dot{x}_8 &= u_5 \,,
\end{aligned}
\tag{8}
$$

$$
\begin{aligned}
\dot{x}_9 = \frac{R x_4}{2F} \Bigg(& \frac{\left(u_1 - \frac{x_8}{2F} M_{\mathrm{H_2}} - k_{\mathrm{a}} \left(x_5 - P_{\mathrm{out,a}}\right)\right) R x_4 + x_1 R \left(\frac{\frac{x_8}{2F} \left|\Delta H\right| - x_8 x_9 - h A_{\mathrm{cool}} \left(x_4 - u_4\right)}{m_{\mathrm{cell}} c_{\mathrm{p,cell}}}\right)}{M_{\mathrm{H_2}} \nu_{\mathrm{a}} x_5} - \frac{u_5}{A_{\mathrm{m}} i_{0,\mathrm{a}} \alpha_{\mathrm{a}}} - \frac{u_5}{2 A_{\mathrm{m}} i_{0,\mathrm{c}} \alpha_{\mathrm{c}}} \\
& + \frac{\left(u_2 - \frac{x_8}{4F} M_{\mathrm{O_2}} - k_{\mathrm{c}} \left(x_6 - P_{\mathrm{out,c}}\right)\right) R x_4 + x_2 R \left(\frac{\frac{x_8}{2F} \left|\Delta H\right| - x_8 x_9 - h A_{\mathrm{cool}} \left(x_4 - u_4\right)}{m_{\mathrm{cell}} c_{\mathrm{p,cell}}}\right)}{2 M_{\mathrm{O_2}} \nu_{\mathrm{c}} x_6} + \frac{u_5}{x_8 - A_{\mathrm{m}} i_{\mathrm{l,a}}} + \frac{u_5}{2 \left(x_8 - A_{\mathrm{m}} i_{\mathrm{l,c}}\right)} \\
& - \frac{\left(u_3 + \frac{x_8}{2F} M_{\mathrm{H_2O}} - k_{\mathrm{c}} \left(x_7 - P_{\mathrm{out,c}}\right)\right) R x_4 + x_3 R \left(\frac{\frac{x_8}{2F} \left|\Delta H\right| - x_8 x_9 - h A_{\mathrm{cool}} \left(x_4 - u_4\right)}{m_{\mathrm{cell}} c_{\mathrm{p,cell}}}\right)}{M_{\mathrm{H_2O}} \nu_{\mathrm{c}} x_7} \Bigg) + \frac{R \left(\frac{\frac{x_8}{2F} \left|\Delta H\right| - x_8 x_9 - h A_{\mathrm{cool}} \left(x_4 - u_4\right)}{m_{\mathrm{cell}} c_{\mathrm{p,cell}}}\right)}{2F} \\
& \left(\ln\left(\frac{x_5 \sqrt{x_6}}{x_7}\right) - \frac{\ln\left(\frac{x_8}{A_{\mathrm{m}} i_{0,\mathrm{a}}}\right)}{\alpha_{\mathrm{a}}} - \frac{\ln\left(\frac{x_8}{A_{\mathrm{m}} i_{0,\mathrm{c}}}\right)}{2\alpha_{\mathrm{c}}} + \ln\left(1 - \frac{x_8}{A_{\mathrm{m}} i_{\mathrm{l,a}}}\right) + \frac{\ln\left(1 - \frac{x_8}{A_{\mathrm{m}} i_{\mathrm{l,c}}}\right)}{2} \right) - \frac{u_5 R_{\Omega}}{A_{\mathrm{m}}} \,.
\end{aligned}
$$

3. DATA COLLECTION AND PARAMETER IDENTIFICATION

The state-space system given by Equation 8 includes numerous unknown parameters. Different parameters are estimated by utilising the collected data from the experiments in an optimisation-based approach. Experimental figures are shown after min-max normalization is applied.

3.1 Experimental Setup and Experiment Design

The Zero Emission Laboratory (ZEL) testbed at MARIN is used for experiments. The setup comprises four 96-cell Nedstack stacks. Twenty seven variables are measured: inlet and outlet pressures and temperatures of anode, cathode, and coolant; stack temperatures; and cell voltages and current. Four inputs are adjustable: current, hydrogen pressure, air stoichiometry, and coolant temperature. As shown in Figure 2, hydrogen pressure and air stoichiometry sweep three levels across three coolant setpoints, while current follows a triangular signal covering the full polarisation range with intermediate flat regions.

3.2 Optimal Parameter Identification

The system includes 11 unknown parameters that can be listed as $\theta = [i_{0,\mathrm{a}}\ i_{0,\mathrm{c}}\ i_{\mathrm{l,a}}\ i_{\mathrm{l,c}}\ E^0\ R_{\Omega}\ k_{\mathrm{a}}\ k_{\mathrm{c}}\ h\ A_{\mathrm{cool}}\ c_{\mathrm{p,cell}}]^T$.

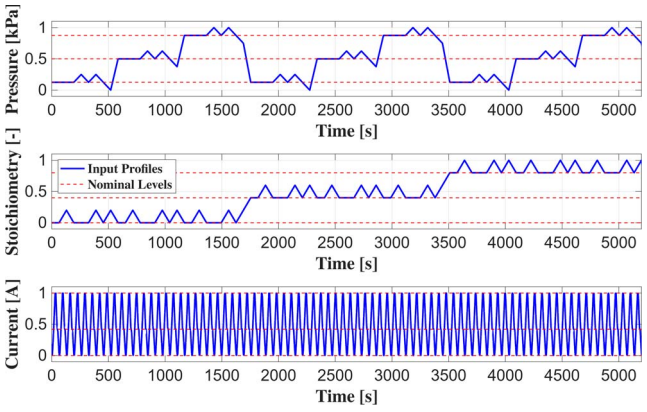


Fig. 2. Input Profiles

The unknown parameters are optimally identified in 3 independent, isolated settings by solving the following optimisation problem, with multiple random initialisations to overcome non-convexity and nonlinearity. The following equation searches for the optimal estimates $f(x;\theta)$ parametrized by θ:

$$
\min_{\theta} \frac{1}{N} \sum_{i=1}^{N} (x_{\mathrm{data}} - f(x;\theta))^2 \,. \tag{9}
$$

The first isolated characteristic is the polarisation curve. The collected data of cell voltages, current, pressures, and cell temperatures are utilized to identify $i_{0,\mathrm{a}}$, $i_{0,\mathrm{c}}$, $i_{\mathrm{l,a}}$, $i_{\mathrm{l,c}}$, E_0 and R_Ω. The approach respects the search space in Santarelli et al. (2006). The problem is solved in an unconstrained way by applying the upper and lower bounds as $10^{-7} \leq i_{0,\mathrm{a}} \leq 0.2$, $10^{-7} \leq i_{0,\mathrm{c}} \leq 10^{-3}$, $0.8 \leq i_{\mathrm{l,a}} \leq 0.9$, $0.8 \leq i_{\mathrm{l,c}} \leq 0.9$, $0 \leq E^0 \leq 1.229$ and $0.15 \leq R_\Omega \leq 0.36$. The resulting polarisation curve in normalised coordinates is shown in Figure 3. The objective function is minimised to 7.712×10^{-5}.

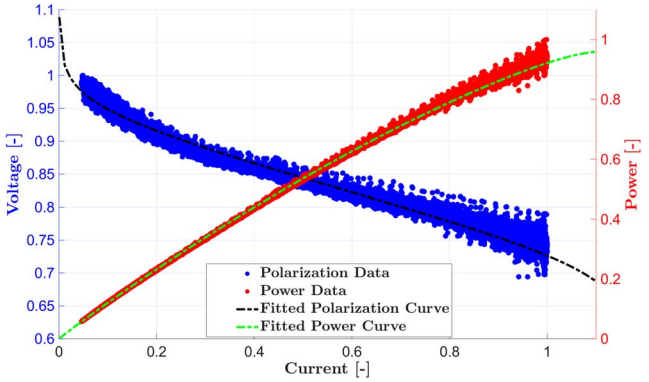


Fig. 3. Polarisation and Power Curve Fitting

The outlet mass flow coefficients are identified next. The linear nozzle parameters k_{a} and k_{c} are fitted using measurements of the stoichiometric flow ratio, inlet and outlet pressures, and the average cell temperature. Cathode parameter identification is straightforward, whereas anode identification is more complex due to the absence of a hydrogen stoichiometry measurement. The Hagen-Poiseuille equation is therefore adopted to represent the anode flow, augmenting the dataset:

$$\begin{aligned} x_{\mathrm{data,anode}} &= 0.95 \frac{\bar{P}\bar{M}}{R\bar{T}} \left(\bar{P} - P_{\mathrm{out,data}}\right) \frac{\pi R_p^4}{8\bar{\mu} L_p} \,, \\ x_{\mathrm{data,cathode}} &= 0.21 \frac{I_{\mathrm{data}}}{4F} M_{\mathrm{O_2}} \lambda_{O_{2,\mathrm{data}}} \,, \end{aligned} \tag{10}$$

where $\bar{P}$, $\bar{T}$, $\bar{M}$, and $\bar{\mu}$ denote the mean pressure, temperature, molar mass (95% H_2 and 21% O_2 are the molar fractions of anode and cathode, respectively), and dynamic viscosity. The pipe radius and length are given by R_p and L_p. The outlet pressures $P_{\mathrm{out,a}}$ and $P_{\mathrm{out,c}}$ are expressed as fitted functions of the inlet partial pressures. Incompressible laminar flow is proven for the system by a pressure drop below 5% on both sides (Figure 4).

As a result, the optimization problem is solved twice for two parameters in an unconstrained way for $[k_{\mathrm{a}}\ k_{\mathrm{c}}] \geq [0\ 0]$. The final objective function values are 2.23×10^{-7} and 4.063×10^{-19} for anode and cathode, respectively.

Finally, the heat transfer characteristics are identified by treating hA_{cool} as a single lumped parameter, optimised jointly with $c_{\mathrm{p,cell}}$. The thermal dynamics are discretised using the Euler method applied to Equation 4, relating the measured average cell temperature across time steps. Due to measurement resolution limitations, the objective function converges to a relatively higher minimum of 1.315.

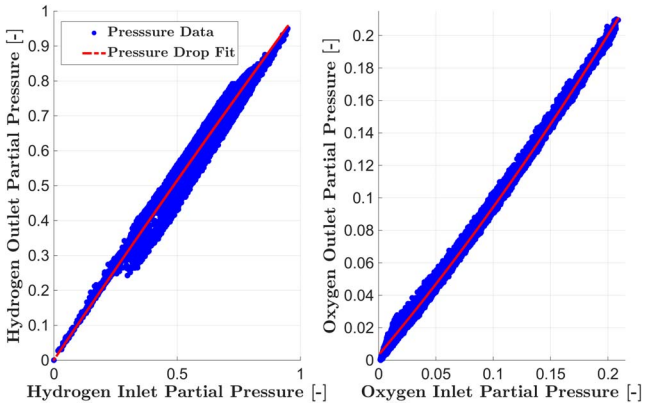


Fig. 4. Outlet Pressure Drop

4. CONTROLLER DESIGN

Candidate control techniques are selected to satisfy the PEM fuel cell operation in maritime settings. Potential challenges of the maritime environment, as well as compatibility with future EMS design, are considered. DFL and ISMC are selected for their ability to handle nonlinearities while maintaining robustness.

4.1 Dynamic Feedback Linearization

DFL cancels model nonlinearities via a coordinate transformation that yields linear dynamics, though it is computationally demanding and sensitive to unmodeled dynamics due to its reliance on Lie derivatives. The design depends on selecting outputs with appropriate relative degrees. For this model, the controller can directly act on 5 states. The state vector is augmented with power output as a tenth state to meet the power demand, without introducing new dynamics. The controlled variables are the partial pressures, cell temperature, and power output, i.e., $h(x) = [x_4\ x_5\ x_6\ x_7\ x_{10}]^T$, each with relative degree 1. Since the total relative degree of 5 is less than the 10 states, exact linearization is not achievable; instead, PFL is applied as a lower-dimensional alternative as follows:

$$\begin{bmatrix} z \\ \eta \end{bmatrix} = \begin{bmatrix} \phi_z(x) \\ \phi_\eta(x) \end{bmatrix} = \begin{bmatrix} h_1(x) \\ L_f h_1(x) \\ \vdots \\ L_f^{r_1-1} h_1(x) \\ h_2(x) \\ L_f h_2(x) \\ \vdots \\ L_f^{r_2-1} h_2(x) \\ \vdots \\ L_f^{r_5-1} h_5(x) \\ \phi_{\eta_1}(x) \\ \phi_{\eta_2}(x) \\ \vdots \\ \phi_{\eta_5}(x) \end{bmatrix} = \begin{bmatrix} x_4 \\ x_5 \\ x_6 \\ x_7 \\ x_{10} \\ x_1 \\ x_2 \\ x_3 \\ x_8 \\ x_9 \end{bmatrix} , \tag{11}$$

where $\phi(x)$ is the coordinate transformation that maps the nonlinear system defined by the coordinates x to a linear space with the coordinates z and to an internal dynamic

space η, r are the relative degrees for each output function. $L_f h(x)$ is the Lie derivative introducing the input–output relations as $L_f h(x) = \frac{\partial h(x)}{\partial x} f(x)$. The input form of the new system is $w = -Q^{-1}(x)(L_f h(x) - u_\ell)$. $Q(x)$ is the decoupling matrix, and $u_\ell = -K(z - z_d)$ is the linear control law for the linear system in z coordinates. The decoupling matrix must be nonzero and invertible to apply the new control law and can be calculated as follows:

$$Q(x) = \begin{bmatrix} L_{g_1} L_f^{r_1-1} h_1(x) & \cdots & L_{g_5} L_f^{r_1-1} h_1(x) \\ L_{g_1} L_f^{r_2-1} h_2(x) & \cdots & L_{g_5} L_f^{r_2-1} h_2(x) \\ \vdots & \ddots & \vdots \\ L_{g_1} L_f^{r_5-1} h_5(x) & \cdots & L_{g_5} L_f^{r_5-1} h_5(x) \end{bmatrix} . \quad (12)$$

Moreover, the system's stability is guaranteed by Lyapunov stability criteria for the linearised dynamics and the zero dynamics. The linearised dynamics stability assessment is done as follows:

$$\begin{aligned} V(z, z_d) &= \frac{1}{2}(z - z_d)^2 , \\ \dot{V}(z, \dot{z}, z_d, \dot{z}_d, u_\ell) &= (\dot{z} - \dot{z}_d)(z - z_d) = -K(z - z_d) . \end{aligned} \quad (13)$$

The form shown in Equation 13 is obtained for all the selected outputs $h(x)$. Therefore, the linearised system is stable. However, the zero dynamics must not show unstable characteristics to ensure global stability. Stability of the zero dynamics is evaluated as follows:

$$\begin{aligned} V(\eta, z, u_\ell) &= \frac{1}{2}(\eta - \eta_d)^2 , \\ \dot{V}(\eta, \dot{\eta}, z, \dot{z}, z_d, \dot{z}_d, u_\ell) &= (\dot{\eta} - \dot{\eta}_d)(\eta - \eta_d) . \end{aligned} \quad (14)$$

Lyapunov stability depends on the selection of the new input gains. It is seen that $\forall\ K \geq 0$, $V(z, z_d) \geq 0$ and $V(\eta, \eta_d) \geq 0$. The stability condition follows $\forall\ K \geq 0$, $\dot{V}(z, z_d, \dot{z}, \dot{z}_d, u_\ell) \leq 0$ and $\dot{V}(z, \dot{z}, z_d, \dot{z}_d, \eta, \dot{\eta}, \eta_d, \dot{\eta}_d, u_\ell) \leq 0$. This shows that both the linearised system and the zero dynamics are globally stable.

4.2 Integral Sliding Mode Controller

ISMC is a robust control technique applicable to nonlinear systems. The controller introduces an additional variable, the sliding surface. For ISMC, the sliding surface of a first-order system is defined as:

$$s = (x - x_d) + \gamma \int_0^t (x(\tau) - x_d(\tau))\, d\tau . \quad (15)$$

The controller comprises two parts: an equivalent action and a switching action. The equivalent action replaces the existing dynamics with the desired dynamics, while the switching action attenuates disturbances. The switching gain must exceed the bounded disturbance amplitude. The input form can be written as $u = g^{-1}(x)\,(f(x) - \dot{x}_d + \gamma(x - x_d) + K\,\mathrm{sign}(s))$. Accordingly, tracking stability is assessed using Lyapunov criteria as follows:

$$\begin{aligned} V(s) &= \frac{1}{2}s^2 , \\ \dot{V}(s, \dot{s}) &= s\dot{s} = -sK\mathrm{sign}(s) = -K|s| . \end{aligned} \quad (16)$$

Equation 16 confirms stability for the partial pressures, cell temperature, and power output, provided the switching gain exceeds the disturbance amplitude. To avoid the chattering effect, $\mathrm{sign}(s)$ is replaced by $\tanh(s)$.

5. SIMULATION RESULTS

Reference states are generated to meet the average cell's power demand. Power information alone is insufficient to define the full state reference; the desired voltage and current are fixed by the identified polarisation curve. The remaining states are calculated to minimise the anode–cathode pressure difference. The following problem is solved in a reduced space for five power demand levels, generating nine state references over 250 s of simulation time:

$$\min_{x_4, x_5, x_6, x_7} \sqrt{\left(\frac{x_5}{0.95} - \frac{x_6}{0.21}\right)^2} . \quad (17)$$

The upper and lower bounds are $325.15 \leq x_4 \leq 353.15$, $101.325 \leq x_5 \leq 506.625$, $101.325 \leq x_6 \leq 506.625$, and $0 \leq x_7 \leq 47.5$. The problem is constrained such that the water partial pressure does not exceed the saturation pressure and the power output matches the demand. Controller performance is evaluated using mean-square tracking error in two cases. The first case considers nominal step power demands representing slow-varying propulsive loads (Figure 5), while the second introduces auxiliary loads as $P_{\text{aux}} \sim \mathcal{N}(0, 8.2807)$, corresponding to ± 5 W fluctuations added each second on top of the first case (Figure 6).

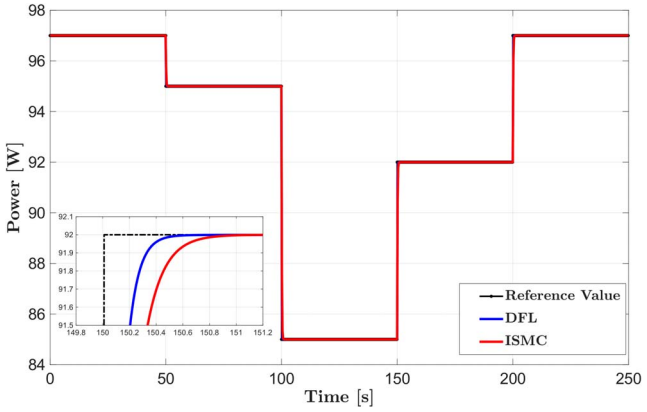


Fig. 5. Controller Performance Case 1

The controller gains are $K_{\text{DFL}} = [15\ \ 10\ \ 10\ \ 10\ \ 13]^T$, $\gamma_{\text{ISMC}} = [10\ \ 7\ \ 7\ \ 7\ \ 8]^T$ and $K_{\text{ISMC}} = [5\ \ 10\ \ 10\ \ 10\ \ 12]^T$. Mean-squared tracking errors for the first case are $e_{\text{DFL}} = 0.025\ W^2$ and $e_{\text{ISMC}} = 0.0414\ W^2$. The response time of DFL is better than ISMC. However, for the second case with the same gains, the mean squared tracking errors are $e_{\text{DFL}} = 1.8219\ W^2$ and $e_{\text{ISMC}} = 1.1229\ W^2$.

6. CONCLUSION

This work presented the development, identification, and control of a dynamic PEM fuel cell model for

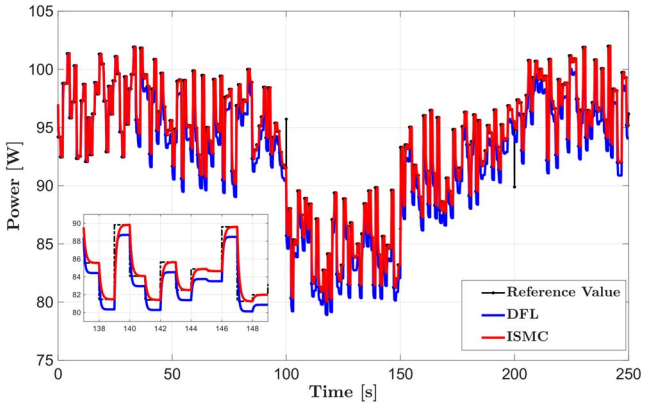


Fig. 6. Controller Performance Case 2

maritime power applications. A physics-based, control-oriented model capturing the coupled electrochemical, thermal, and flow dynamics was formulated, and its parameters were identified using experimental data. Two nonlinear control strategies, PFL and ISMC, were designed for power demand tracking. Instead of addressing a subsystem of the PEM fuel cell dynamics, candidate controllers aimed to control most of the variables in a centralised way. Simulation results confirmed accurate and stable performance under both nominal and aggressive load profiles. PFL exhibited faster transient response and lower steady-state error, while ISMC offered superior robustness to disturbances. Future work will focus on integrating battery storage and developing an EMS for optimal power sharing in hybrid shipboard applications.

REFERENCES

Alireza Abaspour, Nasrin Tadrisi Parsa, M.S. (2014). A new feedback linearization-NSGA-II based control design for PEM fuel cell. *International Journal of Computer Applications*, 97(10), 25–32.

Chatrattanawet, N., Hakhen, T., Kheawhom, S., and Arpornwichanop, A. (2017). Control structure design and robust model predictive control for controlling a proton exchange membrane fuel cell. *Journal of Cleaner Production*, 148, 934–947.

Coraddu, A., Kalikatzarakis, M., Walker, J., Ilardi, D., and Oneto, L. (2022). Chapter 7 - data science and advanced analytics for shipping energy systems. In F. Baldi, A. Coraddu, and M.E. Mondejar (eds.), *Sustainable Energy Systems on Ships*, 303–349. Elsevier.

Coraddu, A., Tamburello, S., Löffler, C., Ceyhun, H.E., van Biert, L., and Oneto, L. (2025). State-of-art energy management strategies for hybrid fuel cell applications for ships. In *Fuel Cell and Hydrogen Technologies in Maritime Transportation*, 121–178. Springer.

Dall'Armi, C., Pivetta, D., and Taccani, R. (2023). Hybrid PEM fuel cell power plants fuelled by hydrogen for improving sustainability in shipping: State of the art and review on active projects. *Energies*, 16(4).

Daud, W., Rosli, R., Majlan, E., Hamid, S., Mohamed, R., and Husaini, T. (2017). PEM fuel cell system control: A review. *Renewable Energy*, 113, 620–638.

Elkafas, A.G., Rivarolo, M., Gadducci, E., Magistri, L., and Massardo, A.F. (2023). Fuel cell systems for maritime: A review of research development, commercial products, applications, and perspectives. *Processes*, 11(1).

Garcia-Gabin, W., Dorado, F., and Bordons, C. (2010). Real-time implementation of a sliding mode controller for air supply on a PEM fuel cell. *Journal of Process Control*, 20(3), 325–336.

IMO, C. (2020). Fourth IMO GHG study 2020. *International Maritime Organization London, UK*.

Kodra, K. and Zhong, N. (2020). Singularly perturbed modeling and LQR controller design for a fuel cell system. *Energies*, 13(11), 2735.

Korkmaz, S.A., Çetinkaya, S.A., Yuksel, O., Konur, O., Erginer, K.E., and Colpan, C.O. (2024). Comparison of various metaheuristic algorithms to extract the optimal PEMFC modeling parameters. *International Journal of Hydrogen Energy*, 51, 1402–1420.

Li, Q., Chen, W., Wang, Y., Jia, J., and Han, M. (2009). Nonlinear robust control of proton exchange membrane fuel cell by state feedback exact linearization. *Journal of Power Sources*, 194(1), 338–348.

Meidanshahi, V. and Karimi, G. (2012). Dynamic modeling, optimization and control of power density in a PEM fuel cell. *Applied energy*, 93, 98–105.

Mylonopoulos, F., Polinder, H., and Coraddu, A. (2023). A comprehensive review of modeling and optimization methods for ship energy systems. *IEEE Access*, 11.

Rabbani, A. and Rokni, M. (2013). Dynamic characteristics of an automotive fuel cell system for transitory load changes. *Sustainable Energy Technologies and Assessments*, 1, 34–43.

Ritzberger, D., Hametner, C., and Jakubek, S. (2020). A real-time dynamic fuel cell system simulation for model-based diagnostics and control: Validation on real driving data. *Energies*, 13(12), 3148.

Ritzberger, D., Höflinger, J., Du, Z.P., Hametner, C., and Jakubek, S. (2021). Data-driven parameterization of polymer electrolyte membrane fuel cell models via simultaneous local linear structured state space identification. *International Journal of Hydrogen Energy*, 46(21), 11878–11893.

Santarelli, M., Torchio, M., and Cochis, P. (2006). Parameters estimation of a PEM fuel cell polarization curve and analysis of their behavior with temperature. *Journal of Power Sources*, 159(2), 824–835.

Van Biert, L., Godjevac, M., Visser, K., and Aravind, P.V. (2016). A review of fuel cell systems for maritime applications. *Journal of Power Sources*, 327, 345–364.

Wang, Y., Yang, X., Sun, Z., and Chen, Z. (2024). A systematic review of system modeling and control strategy of proton exchange membrane fuel cell. *Energy Reviews*, 3(1), 100054.

Zhang, J., Wang, Y.X., He, H., and Wang, Y. (2020). Active thermal management for an automotive water-cooled proton exchange membrane fuel cell by using feedback control. In *2020 IEEE Vehicle Power and Propulsion Conference (VPPC), Gijon, Spain*, 1–5.

Ziogou, C., Voutetakis, S., Georgiadis, M.C., and Papadopoulou, S. (2018). Model predictive control (MPC) strategies for PEM fuel cell systems–a comparative experimental demonstration. *Chemical Engineering Research and Design*, 131, 656–670.